Journal of Power Sources 191 (2009) 217–224

Contents lists available at ScienceDirect

Journal of Power Sources

journal homepage: www.elsevier.com/locate/jpowsour

Performance of lanthanum strontium manganite electrodes at high pressure

E.C. Thomsen, G.W. Coffey, L.R. Pederson*, O.A. Marina

Pacific Northwest National Laboratory, PO Box 999, Richland, WA 99352, USA

ARTICLE INFO

Article history:
Received 19 February 2009
Accepted 19 February 2009
Available online 4 March 2009

Keywords:
Lanthanum manganite
LSM
Cathode
Oxygen electrode
Pressure
Solid oxide fuel cell (SOFC)

ABSTRACT

The high-pressure performance of lanthanum strontium manganite (LSM), LSM–zirconia, and LSM/ceria composite electrodes was studied by impedance spectroscopy and dc methods. Electrode resistances decreased in proportion to $P(O_2)^{1/2}$ for the LSM electrode in both cathodic and anodic directions to at least 10 MPa (~100 atm), a decrease that was attributed to dissociative oxygen adsorption and related phenomena. For the LSM-20/zirconia composite electrode, resistances decreased in proportion to $P(O_2)^{1/4}$ across the entire pressure range considered. Two principal features appeared in the impedance spectra, one that showed a $P(O_2)^{1/4}$ dependence attributed to charge transfer reactions, and a smaller feature that was nearly pressure-independent, possibly due to transport in the zirconia portion of the composite. For the LSM-20/ceria composite electrode, resistances decreased as $P(O_2)^{0.3-0.4}$ at high pressure, depending on temperature. Two features appeared in the impedance spectra: one at low to intermediate frequency having a $\sim P(O_2)^{1/2}$ dependence and a second at high frequency having a $\sim P(O_2)^{1/4}$ dependence. These features are attributed to dissociative oxygen adsorption and to charge transfer reactions, respectively. Results suggest that cathodic losses can be substantially lowered by operation of solid oxide fuel cells at greater than ambient pressure.

1. Introduction

A combination of solid oxide fuel cell (SOFC) and coal gasifier technologies, both of which are being developed with funding from the U.S. Department of Energy, is expected to produce electricity at greater than 50% efficiency (higher heating value or HHV) even with carbon sequestration [1–4]. When the high-temperature exhaust gas from an SOFC system is used to drive a gas turbine, which would minimally affect fuel consumption, efficiencies greater than 65% have been projected [5–9]. An SOFC/GT hybrid may require that the fuel cell operate at above ambient (i.e., 3–15 atm) pressures to provide useful input into the turbine [10–13].

SOFC performance has been shown to improve when operated at pressures above ambient [10–15], where the extent of improvement was greater than expected simply from an increased Nernst potential. The cathode often limits the performance of SOFCs, especially for cell designs having very thin electrolytes [16], and so offers the greatest opportunity for improvement. For a cathode-supported tubular fuel cell having an acceptor-doped lanthanum manganite cathode and operated up to 1 MPa (~10 atm), Virkar et al. [15] concluded that a decrease in cell resistance with pressure primarily was the result of lowered cathodic concentration polarization, which was modeled with a $P(O_2)^{-1}$ dependence. In electrochemical impedance spectroscopy studies with electrolyte-supported symmetric cells with lanthanum strontium manganite (LSM) electrodes, Drevet et al. [17,18] found that electrode polarization decreased with increased oxygen partial pressure up to ~2 MPa, which was attributed to a pressure-induced increase in oxygen ion transport through the cathode lattice. No further changes in electrode performance were reported for pressures greater than ~2 MPa [17,18].

In this study, the performance of $(La_{0.8}Sr_{0.2})_{0.98}MnO_3$ (LSM-20), LSM-20/samaria-doped ceria composite, and LSM-20/yttria-stabilized zirconia (YSZ) composite oxygen electrodes were investigated as a function of oxygen partial pressure from 0.1 to nearly 10 MPa, a pressure range for which very few experimental data are available. LSM is perhaps the best known SOFC oxygen electrode, and is favored because of its good thermal expansion match to YSZ, good stability, high electrical conductivity and good electrocatalytic activity [16,19,20]. LSM is primarily an electronic conductor with minimal ionic conductivity [21], such that the electrode charge transfer resistance scales as the triple-phase boundary length [22]. Composites of LSM with YSZ [23–25] and with ceria [26–30] provide better electrode performance than porous LSM alone. The aim of this study is to provide electrode performance information at high pressures that can be used to develop more accurate models of SOFC/coal gasifier/gas turbine systems as well as in systems where electrochemical compression is being considered.

* Corresponding author. Tel.: +1 509 375 2731; fax: +1 509 375 2167.
E-mail address: larry.pederson@pnl.gov (L.R. Pederson).

0378-7753/$ – see front matter © 2009 Elsevier B.V. All rights reserved.
doi:10.1016/j.jpowsour.2009.02.057

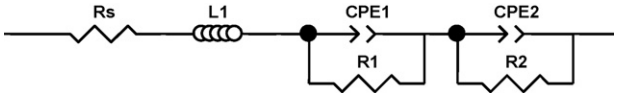

Fig. 1. Equivalent circuit model used to fit impedance spectra.

2. Experimental

Three electrode compositions were considered in this study: (1) $(La_{0.8}Sr_{0.2})_{0.98}MnO_{3+\delta}$ or LSM-20, (2) a 50:50 vol.% composite of LSM-20 and $(Y_2O_3)_{0.08}(ZrO_2)_{0.92}$, and (3) a 50:50 vol.% composite of LSM-20 and $(Sm_2O_3)_{0.20}(CeO_2)_{0.80}$. Materials were prepared using glycine–nitrate combustion synthesis [31]. Nitrate salt stock solutions of lanthanum, strontium, manganese, and iron were standardized by gravimetric and/or complexiometric methods, and then verified by inductively coupled plasma spectroscopy. After combustion, the resulting ash was calcined in air at 1200 °C for 2 h, followed by attrition milling to reduce the average particle size to <1 μm.

Electrode inks were prepared by combining attrition-milled powders with Heraeus V-006 binder in a 50:50 mixture in an Exakt 11671 three-roll mill. These inks were screen printed onto 8% yttria–zirconia (DKKK 8YSZ) pellets that typically were 12 mm in diameter and 2 mm in thickness. A 2 μm-thick samaria–ceria interlayer was applied to minimize electrode interactions with the 8YSZ electrolyte. Identical electrode compositions comprised both the working and counter electrodes, which were sintered at 1100 °C for 2 h. The cell design incorporated a Luggin-type gold reference electrode located approximately half-way through the thickness of the electrolyte [32]. Platinum reference electrodes could not be used because oxidation occurred at high oxygen partial pressures. Contact to the working electrode was made with a gold grid.

A high pressure cell was constructed using a 2 l Parr Instruments™ stainless steel pressure vessel, capable of attaining pressures to 13 MPa. A heating unit to accommodate an electrochemical cell was constructed to fit entirely within the pressure vessel. Electrode performance was evaluated by dc voltammetry, dc current interrupt methods, and electrochemical impedance spectroscopy, using a Solartron™ Model 1260 Frequency Response Analyzer and Model 1287 Electrochemical Interface. Spectra were obtained using an ac amplitude of 15 mV. Impedance spectra were fit to an equivalent circuit model shown in Fig. 1 using ZPlot/ZView software [33]. The model consists of a series resistance that represents the contribution of the zirconia electrolyte, a series inductance that largely arises from electrical leads, and two constant-phase elements in parallel with a resistance, the latter of which represent electrodic processes.

3. Results

3.1. LSM-20 electrode polarization studies

3.1.1. dc results

Current–potential responses for an LSM-20 oxygen electrode on a YSZ electrolyte were obtained at 750 and 850 °C in the oxygen partial pressure range of 0.1 to nearly 10 MPa. Results obtained at 750 °C are shown in Fig. 2. These polarization results were obtained by current interrupt methods to eliminate ohmic losses associated with the relatively thick electrolyte. Current densities corresponding to a given polarization loss in both cathodic and anodic directions continued to increase as the oxygen partial pressure was increased throughout the pressure range considered. No evidence of the existence of a limiting pressure, above which no further improvement occurred, was observed. Polarization curves were fit to the

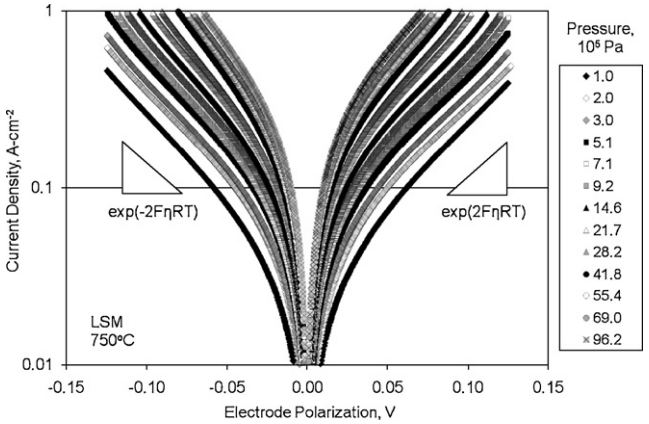

Fig. 2. Current density versus polarization loss for an LSM-20 electrode on a YSZ electrolyte at the indicated oxygen pressures at 750 °C, measured using current interrupt methods.

Butler–Volmer equation [34]:

$$\frac{I}{I_o} = \exp\left(\alpha_a \frac{F\eta}{RT}\right) - \exp\left(-\alpha_c \frac{F\eta}{RT}\right), \quad (1)$$

where I, I_o, α_a, α_c, F, η, R, and T are current density, exchange current density, anodic charge transfer coefficient, cathodic charge transfer coefficient, Faraday constant, overpotential, gas constant, and temperature (K), respectively. The oxygen partial pressure dependence of electrode polarization often is evaluated as a means of obtaining information on the nature of rate-determining steps, represented by

$$R_{el} = k(P_{O_2})^{-n}, \quad (2)$$

where R_{el} is the electrode resistance and k is a rate constant. At low electrode polarization, the electrode resistance and equilibrium exchange currents are related by

$$R_{el} = \frac{\eta}{I} = \frac{1}{I_o} \quad (3)$$

Within experimental error, charge transfer coefficients α_a and α_c remained unchanged as the oxygen partial pressure was increased, with $\alpha_a = 1.9 \pm 0.2$ and $\alpha_c = 2.0 \pm 0.3$ at 750 °C, and with $\alpha_a = 2.2 \pm 0.3$ and $\alpha_c = 2.0 \pm 0.3$ at 850 °C. At the highest oxygen pressures, especially at 850 °C where the entire Butler–Volmer polarization curve could not be established because of experimental current density limitations, charge transfer coefficients α_a and α_c were assumed to be 2.0 for the purpose of calculating exchange current densities. Exchange current densities I_o were found to increase approximately as the square root of the oxygen partial pressure ($n = 1/2$) at both 750 and 850 °C, as is shown in Fig. 3. Exchange currents in anodic and cathodic directions were experimentally indistinguishable.

3.1.2. Electrochemical impedance results

Electrochemical impedance spectra were obtained for each combination of temperature and oxygen partial pressure included in dc measurements. Nyquist and Bode plots for the LSM-20 oxygen electrode at different oxygen partial pressures at 750 °C are given in Fig. 4; similar trends were observed at 850 °C. These spectra correspond to open-circuit conditions, which are comparable to the reciprocal of equilibrium exchange currents determined by dc methods. The width of impedance arcs in Nyquist plots provide a measure of electrodic resistance, and decreased in magnitude with increased pressure at both temperatures, similar to dc results. The ohmic resistance remained unchanged, as expected, represented by a high frequency intercept that was independent of pressure. Impedance spectra appeared to consist of two unresolved arcs, each representing one or more electrodic processes. The presence of at

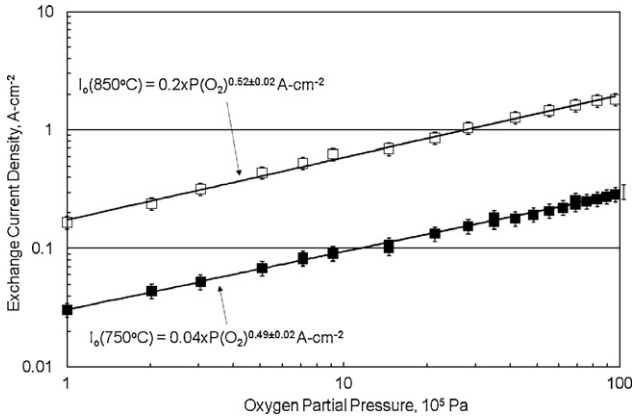

Fig. 3. Oxygen partial pressure dependence of the exchange current density for an LSM-20 electrode at 750 and 850 °C.

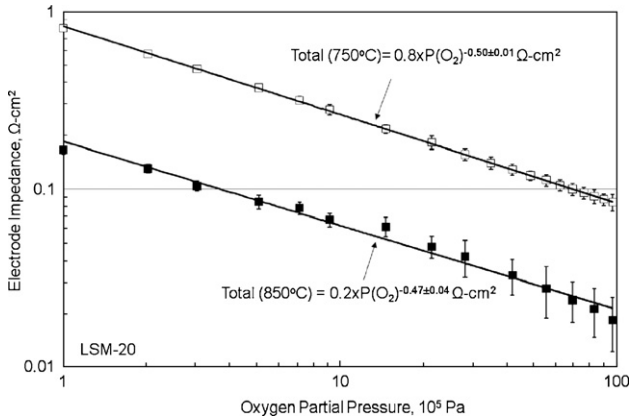

Fig. 5. Oxygen partial pressure dependence of polarization resistance for an LSM-20 electrode on a YSZ electrolyte, obtained at open circuit from electrochemical impedance spectra.

least two arcs was most visible at low temperatures and low oxygen partial pressures, which is consistent with previous observations [35].

Impedance spectra were fit with the equivalent circuit model shown in Fig. 1, to obtain corresponding electrodic resistances as a function of temperature and oxygen partial pressure. Results of these fits, given in Fig. 5, show that electrodic contributions decreased approximately as $P(O_2)^{1/2}$ throughout the experimental pressure range, which is consistent with trends in exchange current densities with pressure measured by dc current interrupt. The two or more suppressed arcs could not be separated reliably, especially at high pressures and high temperatures where the features were very small, so results shown in Fig. 5 are given only as the sum of all electrodic contributions.

3.2. LSM-20/YSZ composite electrode polarization studies

3.2.1. dc results

Current densities for an LSM-20/YSZ composite electrode increased with increased oxygen partial pressure in the range of 0.1–6 MPa, shown in Fig. 6 for tests performed at 800 °C. Current densities in anodic and cathodic directions were similar, as was found for LSM-20 electrodes. Charge transfer coefficients and exchange currents were calculated from the results of Fig. 6, using Eq. (1). The anodic charge transfer coefficient α_a was estimated to be 1.0 ± 0.2 from polarization curves obtained at pressures $\leq$0.5 MPa. This value was used in the calculation of exchange current densities at higher pressures, where practical current limitations prevented the complete polarization curve from being established. The cathodic charge transfer coefficient α_c calculated from polarization curves collected at 5 MPa and lower was 1.2 ± 0.2, which is indistinguishable from results from anodic polarization.

As with LSM, calculated exchange current densities I_o increased continuously with increased oxygen partial pressure, though less quickly than found for LSM-20. As shown in Fig. 7, the exchange current followed a $P(O_2)^{0.26 \pm 0.02}$ dependence at 800 °C. Exchange currents in anodic and cathodic directions were experimentally indistinguishable.

3.2.2. Electrochemical impedance results

Impedance spectra obtained under open circuit conditions for an LSM-20/YSZ composite electrode, given in Fig. 8, reveal at least two features that show quite different oxygen partial pressure dependencies. The feature at low frequency diminishes considerably with increased pressure, while the feature at high frequency shows little change over the same pressure range. These spectra were fit to the equivalent circuit model of Fig. 1, the results of which are given in Fig. 9. The overall resistance determined by impedance

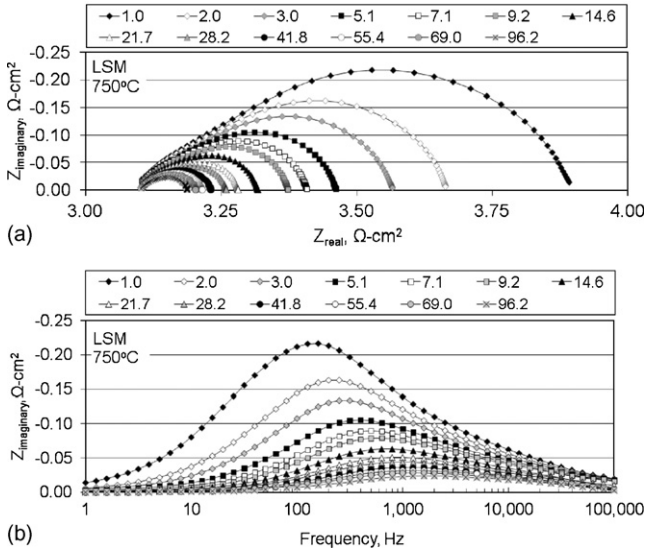

Fig. 4. Electrochemical impedance spectra for an LSM-20 electrode on a YSZ electrolyte at 750 °C under open circuit conditions at the indicated oxygen pressure (10^5 Pa). (a) Nyquist plot and (b) Bode plot.

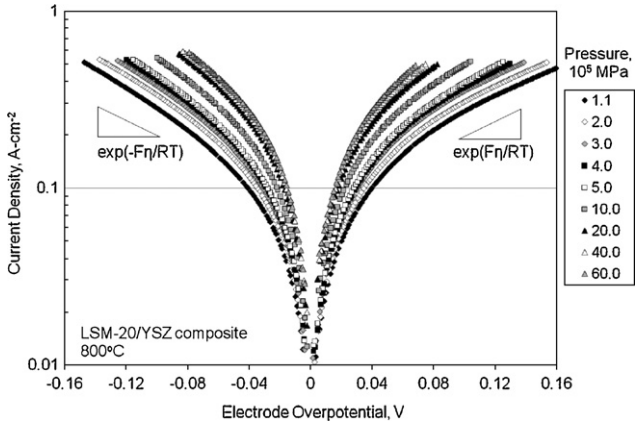

Fig. 6. Current density versus polarization loss for an LSM-20/YSZ composite electrode on a YSZ electrolyte at 800 °C at the indicated oxygen pressures, measured using current interrupt methods.

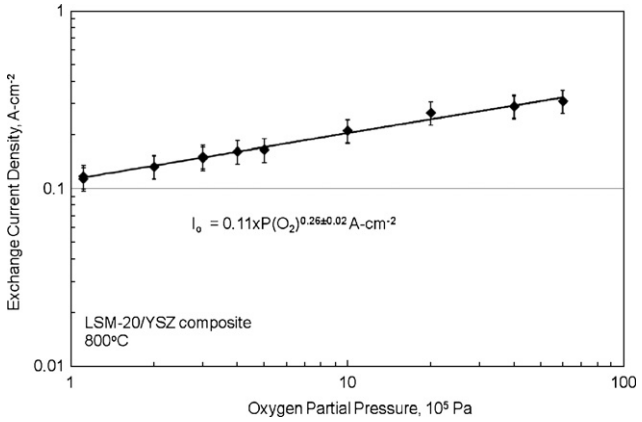

Fig. 7. Exchange current density versus oxygen partial pressure for an LSM-20/YSZ composite electrode on a YSZ electrolyte at 800 °C.

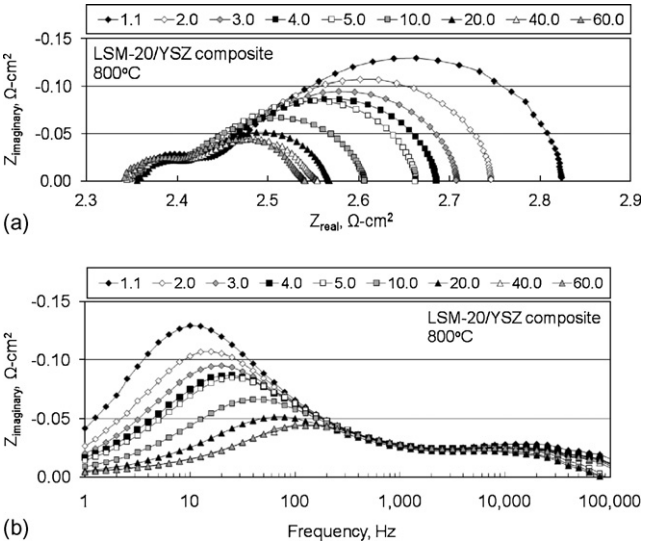

Fig. 8. Electrochemical impedance spectra for an LSM-20/YSZ electrode on a YSZ electrolyte at 800 °C under open circuit conditions at the indicated oxygen pressure (10^5 Pa). (a) Nyquist plot and (b) Bode plot.

spectroscopy followed a $P(O_2)^{0.24\pm0.02}$ dependence, which is in good agreement with the dc results. Fitted results for the low-frequency feature followed a $P(O_2)^{0.28\pm0.03}$ dependence, which cannot be distinguished from the overall pressure dependence.

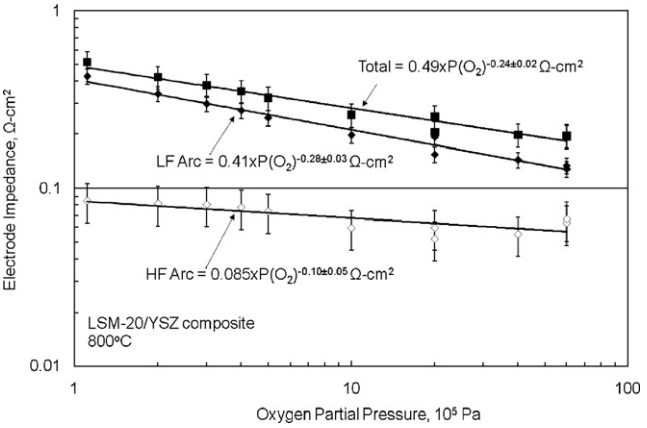

Fig. 9. Oxygen partial pressure dependence of polarization resistance for an LSM-20/YSZ composite electrode obtained at open circuit from electrochemical impedance spectra.

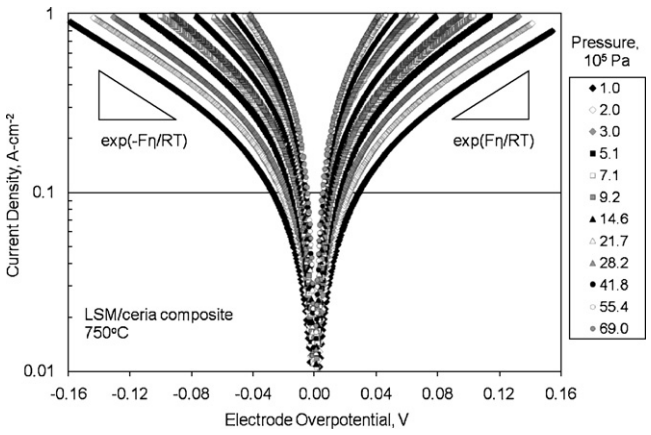

Fig. 10. Current density versus polarization loss for an LSM-20/SDC composite electrode on a YSZ electrolyte at 750 °C at the indicated oxygen pressures, measured using current interrupt methods.

The high-frequency feature followed a $P(O_2)^{0.10\pm0.05}$ dependence, nearly independent of oxygen partial pressure.

3.3. LSM-20/SDC composite electrode polarization studies

3.3.1. dc results

Current densities for a LSM-20/SDC composite electrode also were found to increase continuously with oxygen partial pressure to at least 0.7 MPa, as is shown in Fig. 10 for results obtained at 750 °C. Similar responses to changes in pressure were observed at 850 °C, though with lower polarization loss. Exchange current densities corresponding to a given polarization loss were considerably higher for this mixed-conducting composite than for LSM-20 alone, as were observed previously in performance studies conducted at considerably lower oxygen partial pressures [26–30]. Current densities in anodic and cathodic directions were indistinguishable, as were found for LSM-20 and LSM/YSZ composite electrodes. Charge transfer coefficients and exchange currents were calculated from polarization curves using Eq. (1). Anodic and cathodic transfer coefficients α_a and α_c were identically 1.1 ± 0.2 at 750 and 850 °C, obtained for oxygen partial pressures ≤ 0.9 and ≤ 0.1 MPa, respectively. This value was fixed in the calculation of exchange current densities corresponding to higher oxygen partial pressures, where practical current limitations prevented the complete polarization curve from being obtained.

Exchange current densities increased continuously with increased oxygen partial pressures at both temperatures, though log–log slopes were not identical. As shown in Fig. 11, the exchange current followed a $P(O_2)^{0.43\pm0.03}$ dependence at 750 °C and a $P(O_2)^{0.34\pm0.04}$ dependence at 850 °C. Exchange currents in anodic and cathodic directions were experimentally indistinguishable.

3.3.2. Electrochemical impedance results

Electrochemical impedance spectra for the LSM/ceria composite electrode also showed a trend of continuously decreasing resistance as the pressure of oxygen was increased. Nyquist and Bode plots for this electrode at 750 °C are shown in Fig. 12, with similar trends observed at 850 °C. Impedance spectra appeared to consist of two features: one at higher frequency usually attributed to charge transfer reactions and one at lower frequency usually attributed to processes such as adsorption, dissociation, and diffusion [24,35–37].

Impedance spectra again fit with the equivalent circuit model of Fig. 1 to obtain corresponding electrodic resistances as a function of temperature and oxygen partial pressure, the results of which are shown in Fig. 13. The oxygen partial pressure dependence of

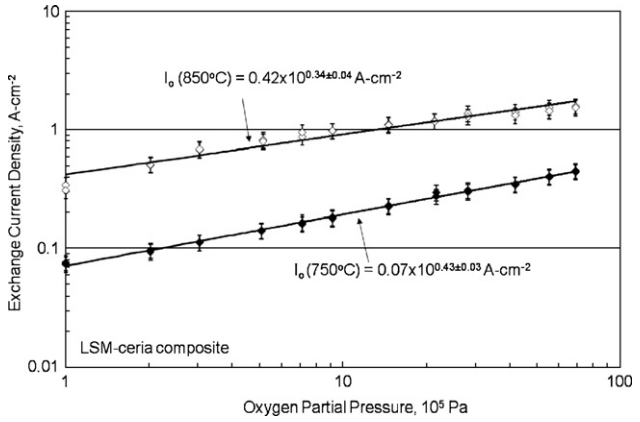

Fig. 11. Exchange current density versus oxygen partial pressure for an LSM-20/SDC composite electrode on a YSZ electrolyte at 750 and 850 °C.

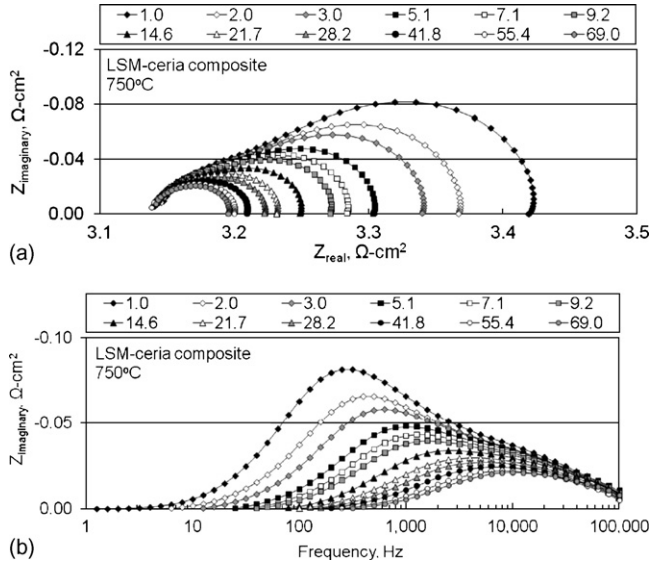

Fig. 12. Electrochemical impedance spectra for an LSM-20/SDC electrode on a YSZ electrolyte at 750 °C under open circuit conditions at the indicated oxygen pressure (10^5 Pa). (a) Nyquist plot and (b) Bode plot.

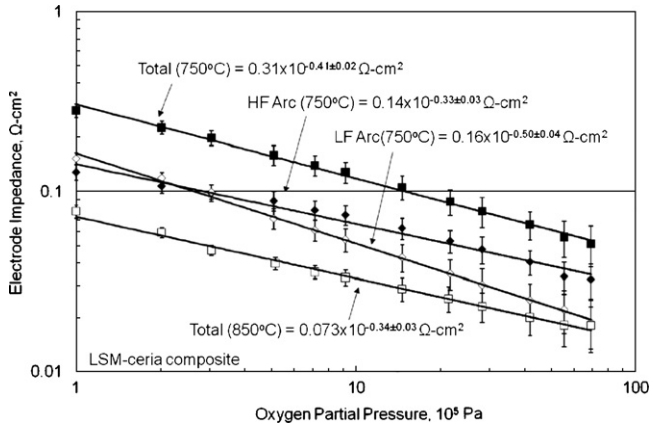

Fig. 13. Oxygen partial pressure dependence of polarization resistance for an LSM-20/SDC composite electrode obtained at open circuit from electrochemical impedance spectra.

the overall polarization resistances was in good agreement with trends in exchange currents determined by dc methods. At 750 °C, the resistance associated with the low-frequency feature showed a $P(O_2)^{0.50\pm0.04}$ dependence, similar to that obtained for the LSM-20 electrode, whereas the high-frequency feature followed a lower $P(O_2)^{0.33\pm0.03}$ dependence. At 850 °C, where the impedance spectra were dominated by the high-frequency feature, the overall electrodic resistance showed a $P(O_2)^{0.34\pm0.03}$ dependence. Though only two features were considered, each arc may represent more than one process, as noted above.

4. Discussion

To summarize findings, exchange current densities varied with oxygen partial pressure from $n = \sim 1/2$ for an LSM-20 electrode to $n = \sim 1/4$ for an LSM-20/YSZ composite over broad ranges of pressure. Intermediate results were observed for an LSM-20/ceria composite electrode, where at least two processes having different oxygen partial pressure dependences were similar in magnitude. Polarization losses in anodic and cathodic directions were essentially identical for each electrode composition. A comparison to the results of previous studies and discussion of possible rate-limiting steps for each electrode system follows.

4.1. LSM-20 electrodes: $P(O_2)^{1/2}$ dependence

Reversible oxygen reduction at the electrode/electrolyte interface can be represented as

$$\frac{1}{2}O_2(g) + 2e' + V_o^{\bullet\bullet} \leftrightarrow O_o^x, \quad (4)$$

where $O_2(g)$, O_o^x, e', and $V_o^{\bullet\bullet}$ are gas-phase oxygen, oxygen in a regular lattice site in the YSZ electrolyte, an electron, and an oxygen vacancy, respectively. At least three successive steps are necessary for oxygen reduction to occur, including oxygen adsorption, diffusion to the active site, and charge transfer, though as many as five different rate-limiting processes may be present [24,35–37]. The reverse (anodic) reaction does not necessarily occur at the same rate as the forward (cathodic) reaction, as different rate-limiting steps may be operative, and anodic and cathodic charge transfer coefficients may neither have the same value nor remain constant with changes in pressure (see Vayenas et al. [38], for example). In this study where electrode polarization was kept relatively low, forward and reverse reactions occurred at similar rates for all three electrodes at all oxygen partial pressures evaluated, implying that the rate-limiting step or steps were similar.

For the LSM-20 electrode, an oxygen partial pressure dependence characterized by $n = 1/2$ has been observed in a number of previous studies, most of which were conducted at pressures below 0.1 MPa. Siebert et al. obtained $n = 0.5$ for single-point electrodes of LSM-10, LSM-30, and LSM-40 in contact with a YSZ electrolyte for oxygen partial pressures in the range 1–10^5 Pa at low electrode polarization, noted to be typical of metallic electrodes [37]. Under high cathodic polarization, a value of $n = 3/8$ was found. Impedance spectra at low polarization were dominated by a single arc with a summit frequency of 10–100 Hz. Siebert et al. concluded that reaction rates were limited by dissociative oxygen adsorption [37]. Tsuneyoshi et al. [39] and Tricker and Stobbs [40] similarly reported $n = 1/2$ for LSM and lanthanum calcium manganite (LCM) electrodes.

Oxygen partial pressure dependences both higher and lower than $n = 0.5$ also have been reported for LSM and LCM electrodes. Murray et al. obtained $n = 0.14$ for an LSM-20 thin film cathode on a single crystal YSZ substrate for oxygen partial pressures less than 0.1 MPa [35]. Impedance spectra obtained in air were dominated by a single arc, with a summit frequency of 100–4000 Hz that

increased with temperature. Results were interpreted as a limiting reaction involving both oxygen adsorption and dissociation. An additional arc was observed at low pressures, with a slope of $n = 0.8$, that was attributed to a diffusion-limiting process [35]. Takeda et al. found $n = 3/4$ for LSM-30 thin film electrodes sputtered onto YSZ at low polarization [41], which also suggests a diffusion-limiting process. Eguchi et al. found two arcs in studies of thin film LSM-40 electrodes on YSZ, of which a low frequency feature was characterized by $n = 1$ (diffusion-limited) and of which the high frequency feature followed $n = 1/4$ (charge transfer-limited) [42]. Virkar et al. concluded from a study of tubular, cathode-supported cell performance at high pressure that concentration polarization ($n = 1$) dominated the performance of the cathode side [15]. The combination of a relatively thick cathode support and operation at practical current densities [15] clearly elevated the importance of concentration polarization contributions relative to electrode kinetics at low polarization. Concentration polarization contributions in this study are eliminated through the use of pure oxygen rather than dilute mixtures and modest current densities.

Drevet et al. studied the performance of LSM-35 electrodes on a YSZ electrolyte to high oxygen partial pressures by impedance spectroscopy in a symmetric cell arrangement at low polarization [17,18]. Their results are consistent with $n = \sim 3/8$ in the oxygen partial pressure range of 0.1–2 MPa, with no further change in electrode performance above $P(O_2) = 2$ MPa. This behavior was attributed to a lowered diffusional resistance at low pressure, transitioning to control by oxygen transport through bulk LSM at high pressure [17,18]. Oxygen mobility in LSM is quite low [43,44], however, in a structure dominated by cation vacancies rather than oxygen ion vacancies [45,46].

For the LSM-20 electrode at low polarization, perhaps the simplest explanation for the observation of $n = 1/2$ over a broad pressure range relates to oxygen adsorption equilibria. Oxygen adsorption may be either associative or dissociative:

$$O_2(g) + \mathrm{ad} \leftrightarrow O_{2-\mathrm{ad}} \quad \text{(associative)} \tag{5}$$

$$O_2(g) + 2\mathrm{ad} \leftrightarrow 2O_{\mathrm{ad}} \quad \text{(dissociative)}, \tag{6}$$

where $O_{2-\mathrm{ad}}$ and O_{ad} represent an adsorbed oxygen molecule and an adsorbed oxygen atom, respectively. Assuming that surface coverage θ can be expressed in the form of a Langmuir isotherm for both the dissociative and associative cases, and assuming that only neutral species are present

$$\frac{\theta_{O_2}}{(1-\theta_{O_2})} = K(P_{O_2}) \quad \text{(associative)} \tag{7}$$

$$\frac{\theta_O}{(1-\theta_O)} = K(P_{O_2})^{1/2} \quad \text{(dissociative)}, \tag{8}$$

where K is the Langmuir constant, and θ_{O_2}, θ_O are coverages of molecular and atomic oxygen, respectively. Observed trends in exchange current densities are consistent with dissociative adsorption Eq. (8), which increases as the square root of oxygen partial pressure for $(1-\theta_O) \gg \theta_O$ Oxygen is believed to be primarily adsorbed dissociatively on LSM [47], and others have concluded that oxygen reduction rates on substituted lanthanum manganite electrodes are limited by dissociative oxygen adsorption [37,39,40]. At high coverage, Eq. (8) also predicts that the amount of oxygen adsorbed will be insensitive to pressure, which was not observed. Insensitivity to pressure also may result if oxygen is adsorbed primarily in forms other than neutral atoms or molecules: Fleig et al. recently showed that the $P(O_2) - \theta$ relation may be flattened considerably if oxygen is present as charged ions, even at low coverages [48]. That $n = 1/2$ holds across a broad pressure range for LSM-20 electrodes in this study implies that surface coverage remains relatively low even to pressures approaching 10 MPa.

4.2. LSM-20/YSZ electrodes: $P(O_2)^{1/4}$ dependence

Composite electrodes comprised of LSM and YSZ offer considerably lower electrode resistances than microporous LSM electrodes alone [23,25,49]. For the LSM-20/YSZ composite electrode examined in this study, overall electrode resistances diminished and exchange currents increased as $n = \sim 1/4$ across a broad pressure range and in both cathodic and anodic directions. This dependence usually is interpreted as evidence for charge transfer as the rate-limiting step. Similar oxygen partial pressure dependences have been obtained in previous studies conducted at much lower pressure. Murray et al. determined $n = 0.29$ for a thin film composite electrode, which was attributed to oxygen dissociation and adsorption as rate-limiting steps [35]. An additional arc was noted in the impedance spectra for the composite electrode in that study, not visible for LSM alone, that showed no oxygen partial pressure dependence. This arc, which increased with increased composite thickness, was attributed to the resistance of YSZ grain boundaries [35]. A similar feature was observed in the present study, with a very small to no dependence on the oxygen partial pressure. Ostergard and Mogensen reported a nearly identical value of $n = 0.3$ for the overall resistance of an LSM/YSZ composite electrode prepared by traditional methods [50]. Kim et al. determined $n = 1/4$ for a series of LSM/YSZ composite electrodes, with a minimum polarization resistance for 40–50 wt.% YSZ [51]. The rate-determining step was attributed to surface diffusion of O^- on LSM [51]. Similarly, Bebelis et al. obtained an oxygen partial pressure dependence of $n = 0.2$ for LSM/YSZ composites for pressures less than 0.1 MPa [26].

Jorgensen and Mogensen identified at least five different processes that affected impedance spectra for LSM/YSZ composite electrodes [24]. At least two steps relate to oxygen ion transport across the LSM/YSZ interface and through YSZ in the composite appear at high frequency, and are expected to have no oxygen partial pressure dependence. A process dominated by dissociative adsorption, surface diffusion, and/or transfer of species at the triple-phase boundary appears at intermediate frequency, with oxygen partial pressure dependences ranging from $n = 0.14$–0.5 based on a literature survey [24]. A process related to diffusion in a stagnant gas layer above the electrode appears at low frequency, with oxygen partial pressure dependences in the range 0.06–0.1 MPa again based on a literature assessment. Finally, an activation process that may be related to the segregation of materials including impurities appears at low frequency, and is expected to be insensitive to the oxygen partial pressure [24]. Of these processes, gas diffusion in a stagnant gas layer is clearly eliminated in this study, because of the use of pure oxygen at high pressure.

Several models have been developed that describe processes consistent with a reaction order of $n = 1/4$. Wang and Nowick developed the following expressions for exchange current densities limited by charge transfer [52]:

$$I_o = C\left[\theta_{\mathrm{ad}}(1-\theta_{\mathrm{ad}})\right]^{1/2} \tag{9}$$

$$I_o = CK^{1/2}\frac{(P_{O_2}^{1/4})}{(1+K(P_{O_2}^{1/2}))}, \tag{10}$$

where C is a constant and K is the Langmuir constant. Eq. (10) correctly yields $n = +1/4$ and $n = -1/4$ for low and high coverages, respectively, for platinum electrodes. Site-limited adsorption effects result in a decrease in oxygen reduction rates with increased pressure for platinum electrodes at high coverage [52], not observed in this work.

Winnubst et al. derived the following expressions for charge transfer-limited exchange current densities for both associative and

dissociative adsorption cases [53]:

$$I_o \approx \theta_o (P_{O_2})^{-\alpha_c/2(\alpha_a+\alpha_c)} = (1-\theta_o)(P_{O_2})^{-\alpha_a/2(\alpha_a+\alpha_c)} \quad \text{(dissociative)} \tag{11}$$

$$I_o \approx \theta_o (P_{O_2})^{-\alpha_c/(\alpha_a+\alpha_c)} = (1-\theta_o)(P_{O_2})^{-\alpha_a/(\alpha_a+\alpha_c)} \quad \text{(associative)} \tag{12}$$

where α_a, α_c are charge transfer coefficients for anodic and cathodic reactions, respectively. If the surface coverage is small such that $(1-\theta) \approx 1$, exchange currents are related to the oxygen partial pressure by [53]:

$$I_o \approx (P_{O_2})^{-\alpha_a/(\alpha_a+\alpha_c)} \quad \text{(dissociative)} \tag{13}$$

$$I_o \approx (P_{O_2})^{-\alpha_a/(\alpha_a+\alpha_c)} \quad \text{(associative)} \tag{14}$$

For the case of $\alpha_a = \alpha_c$, consistent with the results of this study, $n = 1/4$ for dissociative adsorption and $n = 1/2$ for associative adsorption at low coverage. At high coverage, $\theta \approx 1$, so exchange currents would be expected to decrease with increased oxygen partial pressure [53]. Again, present results are more consistent with low rather than high oxygen coverage. Observations that $n = 1/2$ for the LSM-20 electrode may be explained by the associative adsorption case and Eq. (14), though previous studies have concluded that oxygen is dissociatively adsorbed on LSM [37,39,40]. A model was proposed by Van Heuveln et al. that also leads to a prediction that $n = 1/4$, in which the transport of a singly charged oxygen adatom from the adsorption site to the triple-phase boundary competes with charge transfer [54]. Though uncertainties remain concerning the mechanism of oxygen reactions on LSM/YSZ composite electrodes, results from the present study are most consistent with a charge transfer-limited reaction involving dissociatively adsorbed oxygen at low coverage, even to high pressures. An additional feature observed in the impedance spectra at high frequency showed a very low oxygen partial pressure dependence, and may result from grain boundary conduction in YSZ, as suggested previously [35].

4.3. LSM-20/SDC composite electrode: oxygen partial pressure dependence between $P(O_2)^{1/4}$ and $P(O_2)^{1/2}$

As for composites with YSZ, LSM/SDC composite electrodes offer considerably improved performance when compared to LSM alone [26–30]. Relatively few data on the oxygen partial pressure dependence of LSM/SDC composite electrode performance are available. The results of a study by Xu et al. [30] performed at ambient pressures and below are in reasonably good agreement with the results of the present study. Three arcs were found in the impedance spectra: (1) an arc at high frequency showed essentially no oxygen partial pressure dependence; (2) an arc at intermediate frequency yielded $n = 0.34$, and (3) an arc at low frequency gave $n = 0.60$ [30]. In the present study at 750 °C, the arc at intermediate frequency was characterized by $n = 0.33$ while that at low frequency gave $n = 0.50$. The high-frequency arc was attributed to oxygen ion transfer from the triple-phase boundary to the electrolyte, the intermediate frequency arc to charge transfer reactions, and the low-frequency arc to diffusion of O^- along the LSM surface [30], following a mechanism first proposed by van Heuveln et al. [54]. For the overall electrode resistance at 750 °C, the oxygen partial pressure dependence calculated from the results of Xu et al. [30] is $n = \sim 0.4$, which is very similar to that determined in this study ($n = 0.41$–0.43).

In the present work, the overall oxygen partial pressure dependence of LSM/SDC electrode resistances ($n = \sim 0.3$–0.4, depending on temperature) was intermediate between that obtained for LSM-20 electrodes ($n = 1/2$) and LSM/YSZ composite electrodes ($n = 1/4$). At 750 °C, impedance spectra showed two principal features: an arc at low frequency yielded an oxygen partial pressure dependence of $n = \sim 1/2$, and an arc at high frequency gave $n = \sim 1/3$. At 850 °C, the low frequency arc diminished in importance, such that the overall resistance gave $n = \sim 1/3$. The low- to intermediate-frequency feature is attributed to some combination of dissociative adsorption and/or transfer of species at the triple-phase boundary, as has been described for LSM [24,35,37,39,40]. Following similar assignments made for LSM and LSM-composite electrodes from studies performed at low pressures [24–26,30,35,51,54], the feature appearing at high frequency is attributed to a charge transfer reaction, possibly in competition with the diffusion of O^-_{ad} species from adsorption sites to the triple-phase boundary, as proposed previously [54]. The relative importance of dissociative adsorption versus charge transfer is not constant with changes in temperature and oxygen partial pressure, among other factors, resulting in variations in observed relations between overall electrodic resistances and oxygen partial pressure.

5. Summary and conclusions

Electrode resistance and exchange current densities have been determined as a function of oxygen partial pressure for LSM-20, LSM-20/YSZ composite, and LSM-20/SDC composite electrodes. Tests were performed in pure oxygen to pressures of nearly 10 MPa, which eliminates concentration polarization contributions from consideration. Results demonstrate that operation at elevated pressures may be an effective means of lowering the cathodic resistance in SOFCs, where cathode losses account for a significant fraction of stack resistances.

For the LSM-20 electrode, resistances decreased in proportion to $P(O_2)^{1/2}$ across a broad pressure range. Electrode resistances determined from cathodic and anodic polarization were essentially identical. Impedance spectra were dominated by a single process, attributed to dissociative oxygen adsorption and related phenomena. For the LSM-20/YSZ composite electrode, resistances decreased in proportion to $P(O_2)^{1/4}$ across the entire pressure range considered. Two principal features appeared in the impedance spectra. An arc appearing at lower frequencies showed a $\sim P(O_2)^{1/4}$ dependence, which was attributed to charge transfer reactions possibly in competition with the diffusion of O^-_{ad} species from adsorption sites to the triple-phase boundary. A second arc appearing at higher frequency showed very low oxygen partial pressure dependence, and may be the result of ion transport in the YSZ portion of the composite. For the LSM-20/SDC composite electrode, resistances decreased as $P(O_2)^{0.3-0.4}$ at high pressure, depending on temperature. Two features appeared in the impedance spectra: one at low to intermediate frequency having a $P(O_2)^{1/2}$ dependence, and one at high frequency having a $P(O_2)^{1/4}$ dependence. These features are attributed to dissociative oxygen adsorption and to charge transfer reactions, respectively.

The result of this research shows that significant improvements in electrochemical performance of an SOFC could result from operation above ambient pressure, from a lowering of the cathodic contribution to overall cell inefficiencies. These gains are in addition to those due to Nernst potential effects. Integration of an SOFC system with a gas turbine may require that the stack be operated at elevated pressures. Of course, the additional cost of stack operation above ambient pressures must be balanced against expected gains in electrochemical performance.

Acknowledgements

The authors appreciate helpful discussions with P. Singh and J.W. Stevenson. Financial support from the U.S. Department of Energy, Office of Fossil Energy, National Energy Technology Laboratory as part of the Solid State Energy Conversion Alliance (SECA) Coal-

Based Systems Core Research Program (Dr. Paul Tortora, contract manager) is gratefully acknowledged. Pacific Northwest National Laboratory is operated by Battelle for the U.S. Department of Energy under Contract AC06-76RLO 1830.

References

[1] U.S. Department of Energy Office of Fossil Energy, FutureGen: Integrated Hydrogen, Electric Power Production and Carbon Sequestration Research Initiative, March 2004.
[2] M.C. Williams, J.P. Strakey, W.A. Surdoval, Int. J. Appl. Ceramic Technol. 2 (2005) 295.
[3] M.C. Williams, J.P. Strakey, W.A. Surdoval, J. Power Sources 143 (2005) 191.
[4] M.C. Williams, J.P. Strakey, W.A. Surdoval, L.C. Wilson, Solid State Ionics 177 (2006) 2039.
[5] E. Achenbach, J. Power Sources 49 (1994) 333.
[6] F. Bevc, Proc. Inst. Mech. Eng. Part A: J. Power Energy 211 (1997) 359.
[7] S. Campanari, J. Eng. Gas Turbines Power Trans. ASME 122 (2000) 239.
[8] S.P. Harvey, H.J. Richter, J. Energy Resour. Technol. Trans. ASME 116 (1994) 305.
[9] T.W. Song, J.L. Sohn, J.H. Kim, T.S. Kim, S.T. Ro, K. Suzuki, J. Power Sources 142 (2005) 30.
[10] S.C. Singhal, 1996 Fuel Cell Seminar, Orlando, FL, 1996.
[11] S.C. Singhal, Fifth Int. Symp. Solid Oxide Fuel Cells (SOFC-V), 1997.
[12] S.E. Veyo, W. Lundberg, 1996 Fuel Cell Seminar, Orlando, FL, 1996.
[13] N.Q. Minh, SECA Coal-Based System Program, 7th Annual SECA Workshop and Peer Review Meeting, Philadelphia, 2006.
[14] R.A. Roberts, J. Brouwer, E. Liese, R.S. Gemmen, J. Eng. Gas Turbines Power Trans. ASME 128 (2006) 294.
[15] A.V. Virkar, K.-Z. Fung, S.C. Singhal, The effect of pressure on solid oxide fuel cell performance. 98/7303 CONF-9704176, U.S. Department of Energy, Federal Energy Technology Center, 1997.
[16] I.EG&G Technical Services, Fuel Cell Handbook, National Energy Technology Laboratory, Morgantown, WV, 2004.
[17] C. Drevet, Vol. Ph.D., Grenoble, 1996.
[18] C. Drevet, M. Henault, J. Fouletier, Solid State Ionics 136 (2000) 807.
[19] N.Q. Minh, Solid State Ionics 174 (2004) 271.
[20] P. Singh, N.Q. Minh, J. International, Appl. Ceramic Technol. 1 (2004) 5.
[21] J.H. Kuo, H.U. Anderson, D.M. Sparlin, J. Solid State Chem. 83 (1989) 52.
[22] R. Radhakrishnan, A.V. Virkar, S.C. Singhal, J. Electrochem. Soc. 152 (2005) A210.
[23] T. Kenjo, M. Nishiya, Solid State Ionics 57 (1992) 295.
[24] M.J. Jorgensen, M. Mogensen, J. Electrochem. Soc. 148 (2001) A433.
[25] M.J.L. Ostergard, C. Clausen, C. Bagger, M. Mogensen, Electrochimica Acta 40 (1995) 1971.
[26] S. Bebelis, N. Kotsionopoulos, A. Mai, D. Rutenbeck, F. Tietz, Solid State Ionics 177 (2006) 1843.
[27] K.F. Chen, Z. Lu, N. Ai, X.J. Chen, J.Y. Hu, X.Q. Huang, W.H. Su, J. Power Sources 167 (2007) 84.
[28] G.S. Godoi, D.P.F. de Souza, Mater. Sci. Eng. B: Solid State Mater. Adv. Technol. 140 (2007) 90.
[29] S.P. Jiang, W. Wang, Solid State Ionics 176 (2005) 1351.
[30] X.Y. Xu, Z.Y. Jiang, X. Fan, C.R. Xia, Solid State Ionics 177 (2006) 2113.
[31] L.A. Chick, L.R. Pederson, G.D. Maupin, J.L. Bates, L.E. Thomas, G.J. Exarhos, Mater. Lett. 10 (1990) 6.
[32] G. Hsieh, T.O. Mason, E.J. Garboczi, L.R. Pederson, Solid State Ionics 96 (1997) 153.
[33] Scribner Associates, Inc., ZPlot/ZView for Windows, Scribner Associates, Inc., 2008.
[34] C. Wagner, Prog. Solid State Chem. 6 (1971) 1.
[35] E.P. Murray, T. Tsai, S.A. Barnett, Solid State Ionics 110 (1998) 235.
[36] R. Barfod, M. Mogensen, T. Klemenso, A. Hagen, Y.L. Liu, P.V. Hendriksen, J. Electrochem. Soc. 154 (2007) B371.
[37] E. Siebert, A. Hammouche, M. Kleitz, Electrochim. Acta 40 (1995) 1741.
[38] C.G. Vayenas, S.I. Bebekusm, I.V. Yentekakis, S.N. Neophytides, Electrocatalysis and Electrochemical Reactors, CRC Press, Boca Raton, FL, USA, 1996.
[39] K. Tsuneyoshi, K. Mori, A. Sawata, J. Mizusaki, H. Tagawa, Solid State Ionics 35 (1989) 263.
[40] D.M. Tricker, W.M. Stobbs, High Temperature Electrochemical Behavior of Fast Ion and Mixed Conductors, Risoe National Laboratory, Denmark, 1993.
[41] Y. Takeda, R. Kanno, M. Noda, Y. Tomida, O. Yamamoto, J. Electrochem. Soc. 134 (1987) 2656.
[42] K. Eguchi, T. Inoue, M. Veda, J. Kaminae, H. Arai, 2nd International Symposium on Solid Oxide Fuel Cells, 1991.
[43] R.A. De Souza, J.A. Kilner, J.F. Walker, Mater. Lett. 43 (2000) 43.
[44] A.V. Berenov, J.L. MacManus-Driscoll, J.A. Kilner, Solid State Ionics 122 (1999) 41.
[45] J. Mizusaki, N. Mori, H. Takai, Y. Yonemura, H. Minamiue, H. Tagawa, M. Dokiya, H. Inaba, K. Naraya, T. Sasamoto, T. Hashimoto, Solid State Ionics 129 (2000) 163.
[46] F.W. Poulsen, Solid State Ionics 129 (2000) 145.
[47] F.H. van Heuveln, H.J.M. Bouwmeester, J. Electrochem. Soc. 144 (1997) 134.
[48] J. Fleig, R. Merkle, J. Maier, Phys. Chem. Chem. Phys. 9 (2007) 2713.
[49] P. Holtappels, M.J. Jorgensen, S. Primdahl, M. Mogensen, C. Bagger, High Temperature Electrochemistry: Ceramics and Metals Riso National Laboratory, Roskilde, Denmark, 1996.
[50] M.J.L. Ostergard, M. Mogensen, Electrochim. Acta 38 (1993) 2015.
[51] J.D. Kim, G.D. Kim, J.W. Moon, Y. Park, H.W. Le, K. Kobayashi, M. Nagai, C.E. Kim, Solid State Ionics 144 (2001) 387.
[52] D.Y. Wang, A.S. Nowick, J. Electrochem. Soc. 126 (1979) 1155.
[53] A.J.A. Winnubst, A.H.A. Scharenborg, A.J. Burggraaf, Solid State Ionics 14 (1984) 319.
[54] F.H. van Heuveln, H.J.M. Bouwmeester, F.P.F. van Berkel, J. Electrochem. Soc. 144 (1997) 126.